Editors' Suggestion | Featured in Physics

Experimental Observation of an Exceptional Surface in Synthetic Dimensions with Magnon Polaritons

Xufeng Zhang,[1,*] Kun Ding,[2] Xianjing Zhou,[1] Jing Xu,[1] and Dafei Jin[1]
[1]Center for Nanoscale Materials, Argonne National Laboratory, Argonne, Illinois 60439, USA
[2]The Blackett Laboratory, Department of Physics, Imperial College London, London SW7 2AZ, United Kingdom

(Received 2 June 2019; revised manuscript received 25 September 2019; published 4 December 2019)

Exceptional points (EPs) are singularities of energy levels in generalized eigenvalue systems. In this Letter, we demonstrate the surface of EPs on a magnon polariton platform composed of coupled magnons and microwave photons. Our experiments show that EPs form a three-dimensional exceptional surface (ES) when the system is tuned in a four-dimensional synthetic space. We demonstrate that there exists an exceptional saddle point (ESP) in the ES which originates from the unique couplings between magnons and microwave photons. Such an ESP exhibits unique anisotropic behaviors in both the real and imaginary parts of the eigenfrequencies. To the best of our knowledge, this is the first experimental observation of ES, opening up new opportunities for high-dimensional control of non-Hermitian systems.

DOI: 10.1103/PhysRevLett.123.237202

An exceptional point (EP) is the singularity of generalized eigenvalue systems[1–3]. It has drawn intensive interests recently in non-Hermitian systems where dissipations are nonzero and play a critical role in the system behavior [4]. At the EP, both eigenstates and eigenvalues of the system coalesce, distinguishing it from diabolic points where only eigenvalues coalesce. EPs have been studied in a wide range of systems, including coupled resonators or waveguides in optical [5–8], microwave [9–12], magnetic [13], or mechanical domains [14,15]. Novel properties have been discovered around or at the EP, ranging from topological mode transfer [14] and asymmetric mode conversion [6,12,16] to extraordinary sensitivities [7,8,17–19] and directional lasing [20].

Nonetheless, the demonstrations of EPs have been limited to isolated points [6–15] or lines of EPs [21–24]. Along with recent focuses on realizing non-Hermitian analogy of important Hermitian concepts, such as the non-Hermitian Fermi arc [25], exceptional rings spawn from Dirac points [21] and Weyl points [26], it is crucial to extend these concepts to higher dimensions. It has been theoretically proposed recently that surfaces of EPs can be obtained in high-dimensional photonic or mechanical systems [27–30], which can enable intriguing physical phenomena. However, realization of such exceptional surfaces (ESs) requires more degrees of freedom and great tunability, which pose a significant challenge for the experimental demonstration.

On the other hand, magnonic polaritons [31–36] have been emerging as a promising platform for non-Hermitian physics [37]. Strong coupling between magnons (quantization of collective spin excitations) and microwave photons has been demonstrated. Different from most recently demonstrated non-Hermitian systems, magnon polaritons couple two resonances of different physical natures: spins and electromagnetic waves. In such systems, the magnon frequency can be tuned by an external magnetic field, while the coupling strength is determined by the geometry. With such prominent flexibility, magnon polaritons provide an ideal solution for experimental realization of ES.

In this Letter, we show using a magnon polariton system with multiple tuning parameters, EPs can form a three-dimensional (3D) ES within a four-dimensional (4D) synthetic space. Synthetic dimensions have recently been introduced to generate novel topological states that are otherwise difficult to realize [38–40]. Our ES can be conveniently tuned in multiple dimensions simultaneously to coalesce into an exceptional saddle point (ESP). Our measurements show that this ESP is anisotropic, with the real and imaginary parts of the eigenfrequencies behaving differently along three synthetic dimensions. This is distinctly different from recent demonstrations in low-dimensional parameter spaces [41], where an EP pair coalesces in a single dimension and forms an EP with anisotropic behavior only in the imaginary part of the eigenfrequencies. The remarkable observation from our work can trigger the study of synthetic dimension EPs in different systems and their applications in topological state transfer and sensing.

Our system consists of a microwave cavity and a magnonic cavity [Fig. 1(a)]. The microwave cavity is a piece of high-dielectric constant printed circuit board (PCB) [42] sealed with metal walls [43]. With a size of $12 \times 1.2 \times 5$ mm^3, the cavity has its TE_{101} resonance at 9 GHz. Such a volume is drastically reduced compared with conventional air-filled 3D microwave cavities because of the high dielectric constant of the PCB. The magnonic cavity is a 400-μm-diameter yttrium iron garnet (YIG) sphere glued on a ceramic rod. It is placed inside a

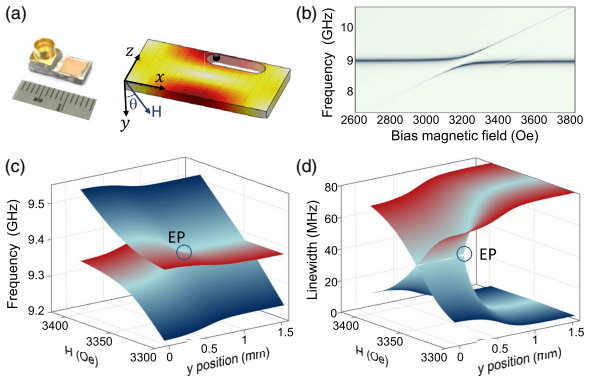

FIG. 1. (a) Picture of the microwave cavity and the simulated cavity magnetic fields for TE_{101} mode (fields inside the slot not shown). A slot is cut near the field maximum to host the YIG sphere. The bias magnetic field is applied in the x-y plane with an angle θ to the y direction. (b) Normalized cavity reflection spectra at different bias fields, showing the anticrossing. The background signals are removed during normalization for clarity. A small anticrossing induced by a high order magnon mode is visible at around 3500 Oe. Slot length: 1 mm. (c),(d) Riemann surfaces for the real (resonance frequency) and imaginary (resonance linewidth) parts of the eigenfrequency, respectively, reconstructed from measured reflection spectra and averaged over multiple measurements. EP is indicated by the circle, showing the bifurcation of the Riemann surface.

1-mm-wide slot on the cavity and can be moved along both x and y directions. The slot length varies in different measurements, causing slight changes in the cavity frequency and magnon-photon coupling strength. A bias magnetic field is applied in the x-y plane with a tunable angle (θ) from the y direction ($\theta = 0$ if not explicitly specified). The magnon mode, i.e., the ferromagnetic resonance of the YIG sphere, is tuned by the magnetic field: $f_m = \gamma H$ where $\gamma = 2.8$ MHz/Oe is the gyromagnetic ratio. When the magnon is tuned to near resonance with the cavity mode, they couple with each other through magnetic dipole-dipole interactions.

The magnon-photon coupling is characterized by measuring the cavity reflection at different H [Fig. 1(b)]. Intrinsic system parameters are extracted via numerical fitting: cavity frequency $f_c = 8.977$ GHz, cavity dissipation $\kappa_c = 54$ MHz, magnon dissipation $\kappa_m = 1.1$ MHz, coupling strength $g = 128$ MHz. Clearly, the magnon-photon coupling dominates over the dissipations of the magnon and cavity photon modes ($g > \kappa_c, \kappa_m$), indicating strong coupling. Despite the large cavity dissipation [43], strong coupling is still achieved because of the significantly reduced cavity volume, which improves the spatial overlap between the photon and magnon modes. The avoided crossing in the spectra also confirms the strong coupling condition. A large cooperativity of $C = g^2/(\kappa_c \times \kappa_m) = 276$ is obtained.

In general, our magnon polariton system can be described by a non-Hermitian Hamiltonian

$$H = \begin{pmatrix} f_c & 0 \\ 0 & f_m \end{pmatrix} + \begin{pmatrix} -i\kappa_c & g \\ g & -i\kappa_m \end{pmatrix}. \quad (1)$$

Solving the Hamiltonian gives two eigenmodes at eigenfrequencies

$$\lambda_\pm = f_\pm + i\kappa_\pm = f_0 + i\kappa_0 \pm \frac{1}{2}\sqrt{(\Delta f - i\Delta\kappa)^2 + 4g^2}, \quad (2)$$

where $f_0 = (f_c + f_m)/2$, $\kappa_0 = (\kappa_c + \kappa_m)/2$, $\Delta f = f_m - f_c$, $\Delta\kappa = \kappa_m - \kappa_c$. The parameters needed for calculating the eigenfrequencies can be extracted from numerical fitting of the cavity reflection spectra [43].

Equation (2) indicates our system has two eigenmodes. The Riemann surfaces in Figs. 1(c) and 1(d) show the real (resonance frequency) and imaginary (linewidth) parts of the eigenfrequencies, respectively, as a function of H and y. These Riemann surfaces are calculated using experiment results and averaged over multiple measurements to eliminate noises and fitting uncertainties [43]. For each (H, y) combination, there are two eigenfrequencies. For large y values, the sphere is far away from the slot and the spatial overlap between magnon and photon modes is small, leading to small g. Therefore, the eigenfrequencies represent the intrinsic magnon and photon modes, with the real part crossing each other at the diabolic points while the imaginary part separating from each other. When y becomes smaller, the sphere is closer to the slot center. The increased mode overlap leads to strong coupling, with avoided crossing in the real part of the eigenfrequencies and mixing of the imaginary part. However, at the onset of the strong coupling ($H = 3348$ Oe, $y = 0.7$ mm), the two eigenfrequencies coalesce into one, corresponding to the singularity condition in Eq. (2), $\Delta f = 0$ and $g = g_c = \Delta\kappa/2$. Such a singularity on Riemann surfaces is referred to as an EP. It is different from the diabolic points which have the same eigenfrequecy but different eigenfunctions. Instead, at the EP, the two eigenfunctions also coalesce into one. Note here only half of the Riemann surface is plotted for clarity. Since moving YIG sphere along either direction of y axis is equivalent, the Riemann surface is symmetric along y axis, and therefore another EP exists at $y = -0.7$ mm.

The multidegree of freedom in our system allows manipulation of EPs in a high-dimensional synthetic space. In addition to the y position of the YIG sphere and the bias field H, the EP condition is also determined by the x position of the YIG sphere. Figure 2(a) plots the measured magnon-photon coupling strength as a function of x and y. The decrease in the coupling strength compared with Fig. 1 is attributed to the extended slot length (5 mm) which gives larger tuning range for g but less confined cavity fields. The saddle-shaped distribution of g is determined by the spatial distribution of the cavity TE_{101} mode inside the slot

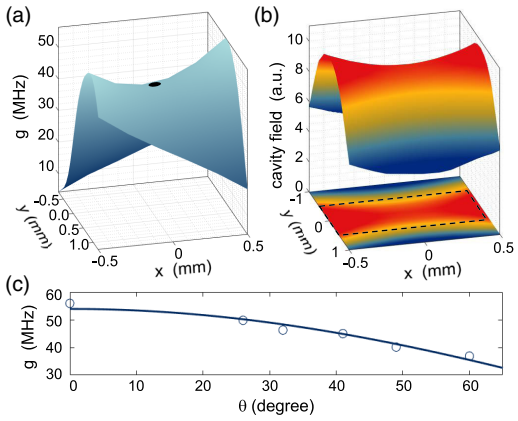

FIG. 2. (a) Coupling strength as a function of x and y. The black dot indicates the saddle point. Slot length: 5 mm. (b) Simulated microwave magnetic field distribution for the cavity mode around the slot. Dashed black line indicates the slot area. (c) Coupling strength as a function of θ at $x = 0$ mm and $y = 0.05$ mm, where θ is the angle of the bias magnetic field relative to the y direction. Circles and the solid line are the measurement and cosine fitting results, respectively.

[Fig. 2(b)]. On the other hand, the coupling strength is also affected by the overlapping factor [31]: $g \propto h \cos\theta$, where h is microwave magnetic field of the cavity mode. Note that the tilted bias magnetic field does not affect the magnon frequency because its amplitude does not change. Figure 2(c) depicts the experimentally observed coupling strength as a function of θ, showing a clear cosine dependence. Therefore, EPs in our system can be tuned in four synthetic dimensions.

These extra dimensions introduce convenient control. Specifically, an EP pair can coalesce into an anisotropic EP [41]. Figures 3(a)–3(c) plot the experimentally obtained Riemann surfaces at different x positions. The slight asymmetry along y is attributed to the perturbation to the cavity cause by the supporting rod of the YIG sphere. The x position of the sphere controls the relative position of the two EPs. When $x = 0.66$ mm, the two EPs are widely separated. As x reduces, they move closer and coalesce at $x = 0.13$ mm. When x keeps decreasing, no EP can be observed (at $x = 0$, e.g.,) and the real part of the two eigenfrequencies always cross each other at diabolic points while the imaginary parts are separated. This can be explained by comparing g for different x positions at a bias magnetic field enabling zero detuning $\Delta f = 0$ [Fig. 3(d)]. When x is large, the maximum of the $g - x$ curve is above the $g = g_c$ line and the two curves cross twice, corresponding to two EPs. Decreasing x also leads to reduced couping strength, moving the whole $g - x$ curve below the $g = g_c$ line and therefore they have no intersections, which consequently eliminates any EPs. At $x = 0.13$ mm, the maximum of the $g - x$ curve is equal to g_c so the two curves is tangent to each other with a single intersection at $y = 0$ mm, corresponding to a single EP.

When an EP pair coalesces, no signature of mode coupling can be observed in the Riemann surface for the real part of the eigenfrequency. However, in the imaginary part, the singularity condition associated with this EP can be easily observed: the top and bottom surfaces are separated from each other but in contact at a single point. A closer examination at this point shows that this coalesced EP behaves differently along the two parameter axises [Figs. 3(e) and 3(f)]. A linear dependence of the linewidth on the y position is obtained near the EP, while for the bias magnetic field it has a square-root dependence. This can be explained by the fact that g has a parabolic dependence on y, while Δf is linearly proportional to H [43].

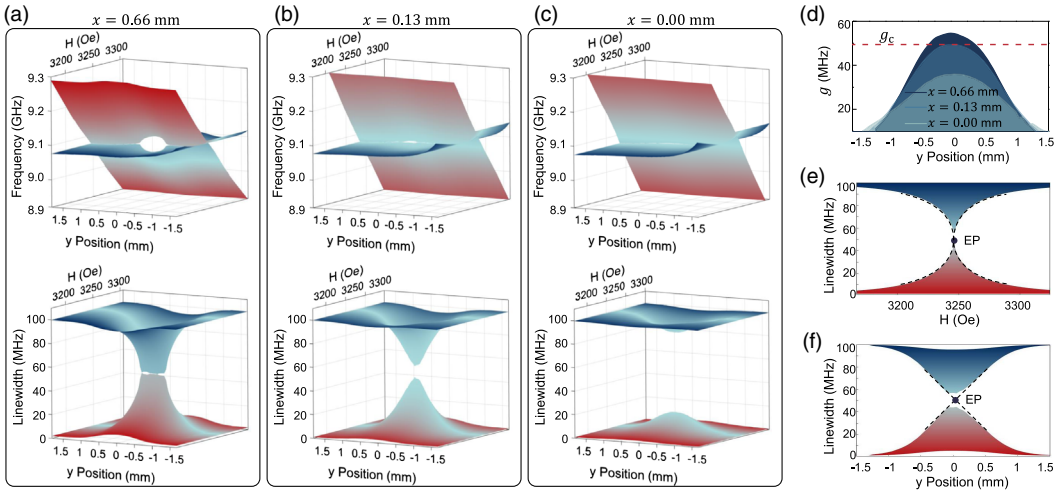

FIG. 3. (a)–(c) Experimentally obtained Riemann surfaces for the real (top) and imaginary (bottom) part of the eigenfrequencies at different x positions of the YIG sphere: $x = 0.66$ mm ($g > g_c$), $x = 0.13$ mm ($g = g_c$), $x = 0.00$ mm ($g < g_c$). EP coalescence is observed at $x = 0.13$ mm when $g = g_c$. (d) Coupling strength g as a function of y positions at various x locations. (e),(f) Cross-sectional views at the EP for the lower figure of (b). Dashed lines are plotted to guide the eye.

However, the EP coalescence only occurs for y. When fixing $y = 0$ and sweeping x, another coalesced EP appears at $x = -0.13$ mm considering the symmetric distribution of g along the x direction [Fig. 2(a)], and these two coalesced EPs form a pair. But within the 4D synthetic space, we can conveniently manipulate the EP pairs to further coalesce them for x positions by taking advantage of the fourth dimension—the magnetic field angle θ.

Figure 4(a) plots the distribution of EPs in the 4D synthetic space (y, x, θ, H). The fourth dimension H is hidden by fixing H at 3237 Oe because EPs always occur at zero detuning ($\Delta f = 0$). The EPs calculated from experimental data are represented by the white dots, while theoretical calculations from extrapolated data are shown in solid lines, and a good agreement is observed. These EPs form an ES which exhibits a saddle-shaped distribution and is in agreement with the relation between the coupling strength and the x and y positions.

EPs always form pairs along either x or y axis on such an ES. However, by varying θ, a unique condition can be found when the EP pair coalesces along both axises. Changing θ effectively changes the overall amplitude of the saddle surface of g. When θ is small (large), g is large (small). Therefore, the saddle surface in Fig. 2(a) intersects the $g = g_c$ plane below (above) the saddle point, and the intersection is a hyperbola with a gap along y (x). At these intersections, $g = g_c$ is satisfied. Therefore, the parameter combination at these intersections (x, y, θ, H) represents the EP condition in the synthetic space, which is summarized in Fig. 4(a). At a critical angle θ_c, the saddle surface intersects the $g = g_c$ plane at the saddle point ($x = x_c$ and $y = y_c$). In this case, the intersection is a single point instead of a hyperbola, indicating the coalescence of EP pairs into one singularity simultaneously in both x and y axis [yellow star in Fig. 4(a)].

The EP coalescence in the 4D synthetic space leads to a nontrivial phenomenon: high-dimensional anisotropic EP. Figures 4(b)–4(d) plot the eigenfrequencies around this ESP. Similar to Fig. 3, the EP coalescence results in anisotropic behavior along y and H axes in the imaginary part of the eigenfrequency. The linewidth shows a linear dependence on y and a square-root dependence on H. While for x, the anisotropic behavior occurs in the real part of the eigenfrequency. A linear dependence on x is observed for the resonance frequency, which shows a square-root dependence on H. Therefore, the ESP is anisotropic along three different synthetic dimensions for both real and imaginary parts of the eigenfrequencies. The linear crossings in both real and imaginary parts of the eigenfrequencies at a single EP are unique to our ESP because of the coupling strength distribution shown in Fig. 2(a). Such carefully designed coupling conditions offer the degrees of freedom to realize other interesting phenomena such as anisotropic high-order EPs in the future. From the application point of view, the resonance frequency and linewidth can be used independently to sense different physical variables with various sensitivities and dynamic ranges.

To summarize, we have experimentally demonstrated the ES in a high-dimensional synthetic space using magnonic polaritons. Such an ES can coalesce to an ESP, leading to the emergence of 3D anisotropic behaviors. Our demonstration shows the great potential of magnon polaritons for high-dimensional non-Hermitian physics and opens up new opportunities. For instance, encircling an EP in the high-dimensional synthetic space can enable new functionalities

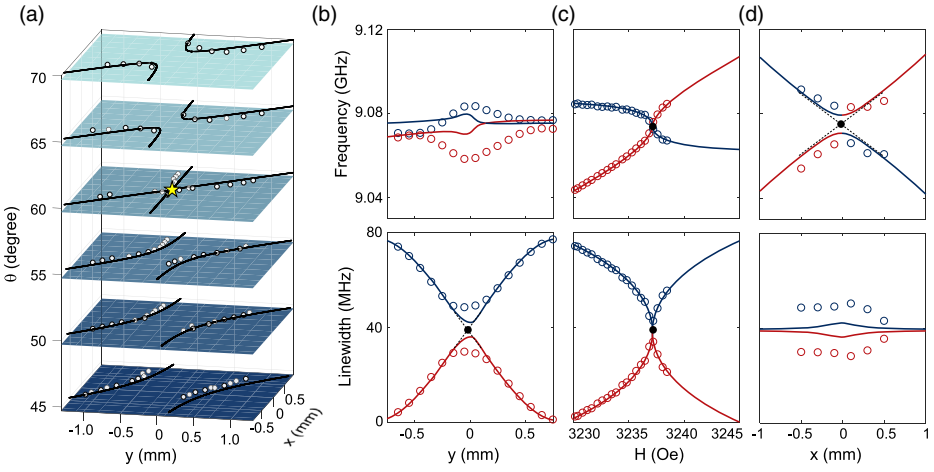

FIG. 4. (a) Slices of ES in the 3D parameter space (x, y, θ). The fourth dimension H is hidden (fixed at $H = 3327$ Oe). White dots: results extracted from experimental data; black lines: calculation from numerical fittings. Planes at given θs are guides to the eye. The yellow star represents the exceptional saddle point. (b)–(d) Cross sections of the Riemann surfaces at the ESP. Top figures: real part of the eigenfrequencies (resonance frequencies). Bottom figures: imaginary part of the eigenfrequencies (linewidth). Circles: experimental results; solid lines: numerical fittings; dashed lines: guides to the eye. Black dots represent EPs. The slight mismatch between experimental results and numerical fittings stems from the imperfect zero-detuning condition ($f_c - f_m \neq 0$) in the experiment.

for topological state transfer or unidirectional propagation. Our work also points out a novel direction for creating high-dimensional EPs. In addition to 3D exceptional surfaces, 4D exceptional volumes or even higher-order EP assembles can be achieved by introducing higher-order synthetic dimensions, which can bring unprecedentedly enriched phenomena in the study of non-Hermitian physics. These demonstrations can also be extended to magnon-based quantum information processing, where the high-synthetic-dimensional control can enable robust quantum state transduction. Therefore, our results lay the groundwork for magnonic non-Hermitian physics and point out a new avenue for magnon-based signal processing.

This work was performed, in part, at the Center for Nanoscale Materials, a U.S. Department of Energy Office of Science User Facility, and supported by the U.S. Department of Energy, Office of Science, under Contract No. DE-AC02-06CH11357. K. D. acknowledges funding from the Gordon and Betty Moore Foundation. X. Z. thanks Dr. Daniel Lopez for enlightening discussions.

*xufeng.zhang@anl.gov

[1] W. D. Heiss, J. Phys. A **37**, 2455 (2004).
[2] M. Batchelor, Z.-M. Li, and H.-Q. Zhou, J. Phys. A **49**, 01LT01 (2016).
[3] Z.-M. Li and M. Batchelor, J. Phys. A **48**, 454005 (2015).
[4] W. D. Heiss, J. Phys. A **45**, 444016 (2012).
[5] M.-A. Miri and A. Alu, Science **363**, eaar7709 (2019).
[6] J. W. Yoon *et al.*, Nature (London) **562**, 86 (2018).
[7] H. Hodaei, A. Hassan, S. Wittek, H. Garcia-Gracia, R. El-Ganainy, D. Christodoulides, and M. Khajavikhan, Nature (London) **548**, 187 (2017).
[8] W. Chen, S. Ozdemir, G. Zhao, J. Wiersig, and L. Yang, Nature (London) **548**, 192 (2017).
[9] C. Dembowski, H. D. Graf, H. L. Harney, A. Heine, W. D. Heiss, H. Rehfeld, and A. Richter, Phys. Rev. Lett. **86**, 787 (2001).
[10] C. Dembowski, B. Dietz, H. D. Graf, H. L. Harney, A. Heine, W. D. Heiss, and A. Richter, Phys. Rev. Lett. **90**, 034101 (2003).
[11] C. Dembowski, B. Dietz, H. D. Graf, H. L. Harney, A. Heine, W. D. Heiss, and A. Richter, Phys. Rev. E **69**, 056216 (2004).
[12] J. Doppler, A. A. Mailybaev, J. Böhm, U. Kuhl, A. Girschik, F. Libisch, T. J. Milburn, P. Rabl, N. Moiseyev, and S. Rotter, Nature (London) **537**, 76 (2016).
[13] X.-L. Zhang, S. Wang, W.-J. Chen, and C. T. Chan, Phys. Rev. A **96**, 022112 (2017).
[14] H. Xu, D. Mason, L. Jiang, and J. Harris, Nature (London) **537**, 80 (2016).
[15] K. Ding, G. Ma, M. Xiao, Z. Q. Zhang, and C. T. Chan, Phys. Rev. X **6**, 021007 (2016).
[16] R. Uzdin, A. Mailybaev, and N. Moiseyev, J. Phys. A **44**, 435302 (2011).
[17] J. Wiersig, Phys. Rev. Lett. **112**, 203901 (2014).
[18] J. Wiersig, Phys. Rev. A **93**, 033809 (2016).
[19] M. Goryachev, B. McAllister, and M. E. Tobar, Phys. Dark Universe **23**, 100244 (2019).
[20] B. Peng, Ş. K. Özdemir, M. Liertzer, W. Chen, J. Kramer, H. Yılmaz, J. Wiersig, S. Rotter, and L. Yang, Proc. Natl. Acad. Sci. U.S.A. **113**, 6845 (2016).
[21] B. Zhen, C. W. Hsu, Y. Igarashi, L. Lu, I. Kaminer, A. Pick, S.-L. Chua, J. D. Joannopoulos, and M. Soljačić, Nature (London) **525**, 354 (2015).
[22] Y. Xu, S.-T. Wang, and L.-M. Duan, Phys. Rev. Lett. **118**, 045701 (2017).
[23] K. Luo, J. Feng, Y. X. Zhao, and R. Yu, arXiv:1810.09231.
[24] A. Cerjan, M. Xiao, L. Yuan, and S. Fan, Phys. Rev. B **97**, 075128 (2018).
[25] H. Zhou, C. Peng, Y. Yoon, C. W. Hsu, K. A. Nelson, L. Fu, J. D. Joannopoulos, M. Soljačić, and B. Zhen, Science **359**, 1009 (2018).
[26] A. Cerjan, S. Huang, M. Wang, K. P. Chen, Y. Chong, and M. C. Rechtsman, Nat. Photonics **13**, 623 (2019).
[27] H. Zhou, J. Y. Lee, S. Liu, and B. Zhen, Optica **6**, 190 (2019).
[28] R. Okugawa and T. Yokoyama, Phys. Rev. B **99**, 041202(R) (2019).
[29] J. C. Budich, J. Carlstrom, F. K. Kunst, and E. J. Bergholtz, Phys. Rev. B **99**, 041406(R) (2019).
[30] Q. Zhong, J. Ren, M. Khajavikhan, D. N. Christodoulides, S. K. Ozdemir, and R. El-Ganainy, Phys. Rev. Lett. **122**, 153902 (2019).
[31] X. Zhang, C.-L. Zou, L. Jiang, and H. X. Tang, Phys. Rev. Lett. **113**, 156401 (2014).
[32] Y. Tabuchi, S. Ishino, T. Ishikawa, R. Yamazaki, K. Usami, and Y. Nakamura, Phys. Rev. Lett. **113**, 083603 (2014).
[33] M. Goryachev, W. G. Farr, D. L. Creedon, Y. Fan, M. Kostylev, and M. E. Tobar, Phys. Rev. Applied **2**, 054002 (2014).
[34] L. Bai, M. Harder, Y. P. Chen, X. Fan, J. Q. Xiao, and C.-M. Hu, Phys. Rev. Lett. **114**, 227201 (2015).
[35] H. Huebl, C. W. Zollitsch, J. Lotze, F. Hocke, M. Greifenstein, A. Marx, R. Gross, and S. T. B. Goennenwein, Phys. Rev. Lett. **111**, 127003 (2013).
[36] B. Bhoi, B. Kim, J. Kim, Y.-J. Cho, and S.-K. Kim, Sci. Rep. **7**, 11930 (2017).
[37] D. Zhang, X.-Q. Luo, Y.-P. Wang, T.-F. Li, and J. You, Nat. Commun. **8**, 1368 (2017).
[38] E. Lustig, S. Weimann, Y. Plotnik, Y. Lumer, M. A. Bandres, A. Szameit, and M. Segev, Nature (London) **567**, 356 (2019).
[39] Q. Wang, M. Xiao, H. Liu, S. Zhu, and C. T. Chan, Phys. Rev. X **7**, 031032 (2017).
[40] L. Yuan, Q. Lin, M. Xiao, and S. Fan, Optica **5**, 1396 (2018).
[41] K. Ding, G. Ma, Z. Q. Zhang, and C. T. Chan, Phys. Rev. Lett. **121**, 085702 (2018).
[42] Rogers Corporation.
[43] See Supplemental Material at http://link.aps.org/supplemental/10.1103/PhysRevLett.123.237202 for details about device preparation, measurement setup, and data processing procedure.